PCCP

PAPER

View Article Online
View Journal

Cite this: DOI: 10.1039/c4cp02405b

Substitution of a hydroxamic acid anchor into the MK-2 dye for enhanced photovoltaic performance and water stability in a DSSC†

C. Koenigsmann,[a] T. S. Ripolles,‡[b] B. J. Brennan,‡[a] C. F. A. Negre,[a] M. Koepf,[a] A. C. Durrell,[a] R. L. Milot,[a] J. A. Torre,[b] R. H. Crabtree,*[a] V. S. Batista,*[a] G. W. Brudvig,*[a] J. Bisquert*[bc] and C. A. Schmuttenmaer*[a]

Received 1st June 2014,
Accepted 10th June 2014

DOI: 10.1039/c4cp02405b

www.rsc.org/pccp

An efficient synthetic protocol to functionalize the cyanoacrylic acid anchoring group of commercially available MK-2 dye with a highly water-stable hydroxamate anchoring group is described. Extensive characterization of this hydroxamate-modified dye (MK-2HA) reveals that the modification does not affect its favorable optoelectronic properties. Dye-sensitized solar cells (DSSCs) prepared with the MK-2HA dye attain improved efficiency (6.9%), relative to analogously prepared devices with commercial MK-2 and N719 dyes. The hydroxamate anchoring group also contributes to significantly increased water stability, with a decrease in the rate constant for dye desorption of MK-2HA relative to MK-2 in the presence of water by as much as 37.5%. In addition, the hydroxamate-anchored dye undergoes essentially no loss in DSSC efficiency and the external quantum efficiency improves when up to 20% water is purposefully added to the electrolyte. In contrast, devices prepared with the commercial dye suffer a 50% decline in efficiency under identical conditions, with a concomitant decrease in external quantum efficiency. Collectively, our results indicate that covalent functionalization of organic dyes with hydroxamate anchoring groups is a simple and efficient approach to improving the water stability of the dye–semiconductor interface and overall device durability.

1. Introduction

There has been considerable recent interest in the development of efficient, durable photoelectrochemical devices with the overarching goal of effectively converting solar energy into electricity and solar fuels.[1–5] Dye-sensitized solar cells (DSSCs) are a particularly promising device architecture owing to their ease of manufacture and relatively low cost in comparison with silicon solar cells.[4,6–9] However, widespread commercialization of DSSCs has been hindered by their poor long-term durability resulting from a variety of degradation processes, especially upon exposure to heat and humidity.[10–12] Several mechanisms leading to performance loss have been identified, including corrosion of the sealing materials, evaporation of the electrolyte solvent, and instability of the sensitizer molecules. Despite improvements in the durability of sealant materials and the use of high boiling point solvents in electrolyte formulations, the degradation of sensitizer molecules continues to be a key technological shortfall.[11]

In DSSCs, mesoporous wide-band gap semiconductor films are sensitized to absorb light in the visible solar spectrum by covalent attachment of inorganic or organic chromophores.[9,13] Under illumination, photoexcitation of the dye results in a rapid interfacial electron transfer (IET) into the conduction band of the semiconductor, leading to charge separation.[14–16] DSSC sensitizers have traditionally relied on a class of inorganic complexes consisting of Ru-polypyridyl frameworks, such as the well-studied N719 [di-tetrabutylammonium *cis*-bis(isothiocyanato) bis(2,2′-bipyridyl-4,4′-dicarboxylato) ruthenium(II)] dye.[17–19] However, the high cost and low earth abundance of noble metals has stimulated interest in a growing class of organic dyes based largely on a donor–linker–acceptor (DLA) structural framework.[20–25] Compared with Ru-based analogs, organic dyes typically have higher absorption coefficients, are considerably less costly, and are relatively easy

[a] *Yale Energy Sciences Institute and Department of Chemistry, Yale University, New Haven, Connecticut, 06520-8107, USA. E-mail: victor.batista@yale.edu, gary.brudvig@yale.edu, robert.crabtree@yale.edu, charles.schmuttenmaer@yale.edu*

[b] *Photovoltaic and Optoelectronic Devices Group, Departament de Física, Universitat Jaume I, 12071 Castelló, Spain*

[c] *Department of Chemistry, Faculty of Science, King Abdulaziz University, Jeddah, Saudi Arabia*

† Electronic supplementary information (ESI) available: Additional details regarding the synthesis, characterization, computational methods and analysis of the desorption data are included. Also presented are additional data involving the TDDFT, spectroscopic, electrochemical and device performance data for the MK-2, MK-2HA, MK-2E and MK-2THP dyes. See DOI: 10.1039/c4cp02405b

‡ These two authors contributed equally to this work.

to synthesize.[22,26] In addition, the ability to tailor the structure of organic dyes has led to advances in solving the inherent challenges of dye aggregation and short lifetimes of the charge-separated state.[23–25] Collectively, over one-hundred examples of organic dyes have been developed that attain reasonable efficiencies in DSSCs.[9]

Organic dyes relevant to DSSCs typically employ a cyanoacrylate moiety which serves as both the electron acceptor and covalent anchor to the metal oxide framework of the semiconductor nanoparticle.[27] In a fashion analogous to Ru-dyes, covalent attachment to the surface is formed by a carboxylate group leading to a bridging bidentate interaction with the surface.[7] The carboxylate linkage affords rapid IET rates that have been measured on the sub-picosecond time scale, leading to efficient electron injection.[28–30] However, the carboxylate linkage, especially in the case of cyanoacrylate linkers, is susceptible to hydrolysis and subsequent detachment of the dye. This renders the dye–semiconductor interface vulnerable to degradation in the presence of trace quantities of water within the electrolyte.[29,31,32] The poor water stability of the interface has necessitated complex manufacturing procedures to exclude moisture, and limits long-term durability due to the water seepage into the electrolyte during operation.[11,33] For example, hydrophobic Ru-dyes have lower than expected performance in water-based electrolytes due to dye desorption, poor wetting of the mesoporous film and high rates of recombination.[34] In the case of organic dyes, recent results by Sun and co-workers have demonstrated in the case of MK-2, a well-studied organic dye, that its desorption from the semiconductor surface is significantly increased by even trace amounts of water.[27] Water stability is also a fundamental concern in the context of developing artificial photosynthetic cells, which by definition operate under completely aqueous conditions.[2,35,36]

Thus, the realization of stable and durable dye–semiconductor interfaces based on organic dyes requires the development of new anchoring moieties that promote favorable electron-transfer kinetics and are stable toward hydrolysis. Recent results from our group suggest that hydroxamate linkers lead to considerable enhancements in water tolerance as a result of their stronger interaction with the surface of TiO_2.[31,32,37,38] On the basis of equally strong binding of their N-aryl derivatives,[39] we now believe that the hydroxamic acid precursor binds in the mono-deprotonated or hydroxamate form, and not the bis-deprotonated hydroximate form that we favored in earlier work.

In this article, we demonstrate for the first time an efficient synthetic protocol to modify the existing cyanoacrylate moiety of organic dyes with a highly water-stable hydroxamate anchoring group *via* a condensation reaction. This approach is particularly advantageous since it is synthetically facile, resulting in high yields, and more importantly, the chemo-selectivity and mild reaction conditions allows wide application of this strategy to the broad range of common organic dyes possessing cyanoacrylate or carboxylate anchoring groups.[9,40] Thus, this approach is broadly applicable in increasing the water stability of the dye–semiconductor interface of organic dyes.

As a prototypical example, we employ the commercially available MK-2 dye since it is well characterized, chemically stable and maintains high performance in DSSC devices. Due to prior results demonstrating the poor durability of the MK-2–TiO_2 interface, we have modified the as-received commercial MK-2 dye with a hydroxamate anchoring group (MK-2HA, Scheme 1) and have performed a systematic investigation of the performance of this dye in comparison with its as-received, commercial analog. Characterization of the modified dye confirms that the opto-electronic properties of the dye, including the high molar absorption coefficient, are retained. DSSCs sensitized with MK-2HA and MK-2 achieved efficiencies of 6.9% and 6.6%, respectively, compared to 6.3% for the commercial N719 dye. Spectroscopic characterization of the DSSC devices and sensitized films reveals that the hydroxamate anchoring of the MK-2HA dye contributes to significant increases in the recombination resistance and lifetime of the charge separated state.

Modification of the MK-2 dye with a hydroxamate anchoring group dramatically improves the water stability. Dye desorption experiments performed in the presence of water confirm that the MK-2HA is significantly less susceptible to desorption than the commercial MK-2 dye. Surprisingly, exposure of the

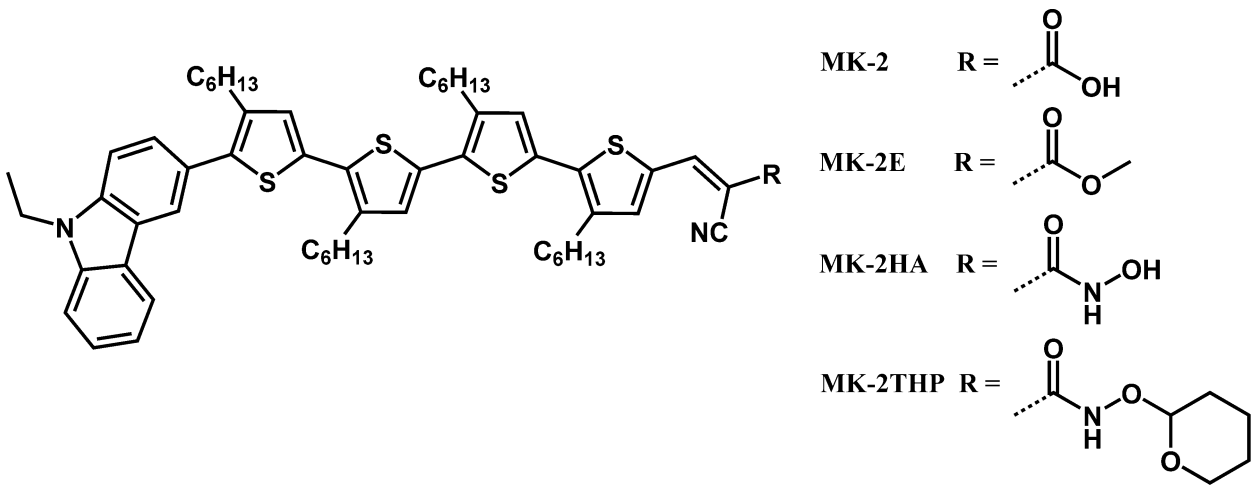

Scheme 1 Structures of the relevant MK-2 analogs.

MK-2HA film to a 1% water–DMF solution results in a 3-fold increase in the lifetime of the charge-separated state with no measurable decrease in the electron injection efficiency. Under operating conditions, DSSC devices prepared with MK-2HA dye suffer essentially no loss in efficiency when water is purposefully incorporated into the electrolyte formulation, whereas devices prepared with the commercial MK-2 dye undergo declines of up to 50% in efficiency with added water. Thus, our functionalization strategy allows for the high photoelectrochemical performance of the MK-2 dye to be retained even in the presence of water.

2. Experimental procedures

2.1 Synthesis & characterization

The synthesis of the MK-2HA dye (Scheme S1, ESI†) is described in detail in the ESI.† In the first step, the commercial MK-2 dye is modified with a protected hydroxylamine species by a peptide coupling reaction carried out at room temperature in dimethylformamide yielding the protected MK-2THP dye. The MK-2THP is deprotected by acetic acid catalyzed hydrolysis, which is performed at 60 °C in an aqueous solution of tetrahydrofuran (THF), to yield the desired MK-2HA. In order to characterize the electrochemical and photophysical properties, we have also prepared the ester form of the commercial MK-2 dye (MK-2E). The esterification of the commercial acid (Scheme S2, ESI†) was accomplished by reacting the commercial MK-2 dye with iodomethane in the presence of potassium carbonate. Details of the characterization including NMR, UV-visible, photoluminescence spectroscopy and mass spectrometry are presented for the MK-2E, MK-2THP, and MK-2HA dyes in the ESI.†

2.2 Characterization of photoelectrochemical performance in dye-sensitized solar cells

Fabrication of DSSCs sensitized with MK-2 and MK-2HA was based on previously reported methods and the details are described in the ESI.†[41] Devices in Section 3.2 were prepared with Electrolyte A (Table 1), which was optimized for the MK-2 dye. However, in Section 3.6, the concentration of DMPII (Electrolyte B) was increased to suitably co-solubilize the electrolyte components with water, which was added to study the stability of the devices. The DSSCs were characterized by electrical methods including current density–voltage (j–V) curves and impedance spectroscopy (IS) under simulated 1 sun irradiation corresponding to AM1.5G (1000 W m^{-2}) sunlight. All measurements were performed without a mask. The measurements were carried out using a PARSTAT 4000 potentiostat (Princeton Applied Research) and a solar simulator equipped with a 1000 W ozone-free Xenon lamp and AM1.5G filter. The light intensity was adjusted with a diode calibrated by Newport to ASTM E948-09 and E1021-06 standards. IS measurements were performed from 0 V to V_{oc} at intervals of 50 mV, using a range of frequencies between 1 MHz to 100 mHz. These data were fitted using the equivalent circuit models for DSSCs proposed by Bisquert and co-workers.[42]

Table 1 DSSC electrolyte formulations

Electrolyte	[DMPII][a]	[LiI]	[I_2]	[TBP][b]
A	0.6	0.1	0.2	0.5
B	2.0	0.1	0.2	0.5

[a] 1,2-Dimethyl-3-propylimidazolium iodide. [b] 4-*tert*-Butylpyridine. Electrolyte solutions were prepared with anhydrous acetonitrile and all concentrations are reported in units of molar (M).

2.3 Spectroscopic characterization of TiO_2 films sensitized with MK-2 and MK-2HA

Transient absorption measurements were performed with a commercial LP920 laser flash photolysis spectrometer (Edinburgh Instruments). Sample excitation was achieved using an optical parametric oscillator (Spectra-Physics basiScan-M, ~1 cm beam diameter, 200 μJ per pulse), pumped by the third harmonic of a Nd:YAG laser (Spectra-Physics Quanta-Ray INDI 40-10, 5–8 ns pulses, operated at 1 Hz). A pulsed 450 W Xe arc lamp provided a white light probe pulse. Transmitted light was focused on a 0.3 m focal length monochromator and detected with a photomultiplier tube (PMT, Hamamatsu R9105). The PMT current was amplified and recorded with a transient digitizer (Tektronix TDS 3032C). A combination of short- and long-pass filters was employed to remove scattered light. Transient absorption measurements were carried out on sensitized TiO_2 films that were placed at a 45° angle in a 1 cm × 1 cm quartz cuvette containing acetonitrile or mixtures of acetonitrile and water. Samples were excited at 560 nm, and single wavelength decays were averaged over 100 laser pulses.

Time-resolved THz spectroscopy (TRTS) measurements were performed following established experimental procedures.[15,43,44] Approximately one quarter of the output of an 4 W amplified Ti:sapphire laser system (Spectra Physics: Mai Tai SP, Empower 30, Spitfire Ace) with a 35 fs pulse duration, 800 nm center frequency, and 1 kHz repetition rate was used for THz generation *via* optical rectification in a ZnTe(110) crystal and THz detection *via* free-space electro-optic sampling in an additional ZnTe(110) crystal. Another quarter of the power was frequency doubled to 400 nm in a β-barium borate (BBO) crystal and dedicated to photoexcitation of the sample. The change in peak amplitude of the time-domain THz pulse was then monitored as a function of its delay with respect to the optical pump pulse to measure the time and efficiency of electron injection. Samples consisted of a 15 μm thick layer of transparent TiO_2 deposited onto 1 mm thick quartz plates (1 cm × 1 cm) according to the methods described in Section 2.2. The quartz was pre-treated before deposition by immersion in a solution consisting of 75% sulfuric acid (Fisher Scientific) and 25% hydrogen peroxide (30 vol% in water, Fisher Scientific) for a period of 30 minutes to improve adhesion of the films.

2.4 Durability and stability testing of TiO_2 films sensitized with MK-2 and MK-2HA

The water stability and durability of TiO_2 films sensitized with MK-2 and MK-2HA were studied by systematically investigating the rate of dye desorption when soaking in solutions of dimethylformamide (DMF, Sigma Aldrich, <0.005% H_2O, 99.8%) and

water (18.2 MΩ cm). MK-2 and MK-2HA sensitized TiO_2 films were prepared with a single 5 μm thick layer of transparent TiO_2 deposited onto TEC15 FTO glass utilizing the procedure described in Section 2.2. The geometric area of the sensitized film was measured from optical images utilizing the ImageJ software.[45] Prior to studying the desorption kinetics, the molar absorption coefficients were determined for MK-2 and MK-2HA in solutions of DMF–H_2O by diluting standardized solutions of the dyes in pure DMF. Subsequently, desorption experiments were performed by immersing the sensitized film into a solution containing 0.1, 0.5, or 1.0 vol% water dissolved in DMF. The time-dependent desorption of the dye was measured *in situ* by UV-visible spectroscopy over the period of 240 min to determine the quantity of dye desorbed into the DMF–H_2O solution. Control experiments were performed on the MK-2 and MK-2HA films by immersing electrodes into anhydrous DMF. In this case, time-dependent desorption of the dye was measured from five discrete sensitized films in separate desorption experiments after 45, 90, 135, 180 and 240 min. Each experiment was performed in tightly sealed vials prepared under Ar, in order to avoid contamination by moisture from the atmosphere. After desorption in DMF–H_2O, the electrodes were blown dry under a stream of nitrogen and placed into a solution consisting of 50 μL of a 1 M tetra-*n*-butylammonium hydroxide (TBAH, 1 M in methanol, Acros Organics) dissolved into 15 mL of THF which thereby desorbed all dye remaining on the surface.

In addition to measuring the rate of dye desorption, the effect of dye desorption on the IET efficiency by was examined by means of TRTS. In this study, as-prepared films were aged at a relative humidity of 85% at room temperature (21 °C) for a period of six days. Subsequently, the films were immersed into solutions of 1% H_2O–DMF for a period of four hours. The IET efficiency determined by TRTS (*cf.* Section 2.3) was measured for the films to determine the effects of aging conditions and desorption.

3. Results & discussion

3.1 Synthesis and characterization of MK-2 and MK-2HA dyes

Modification of commercial MK-2 dye with a hydroxamate anchoring group was accomplished in two synthetic steps. The structures of the relevant MK-2 analogs are provided in Scheme 1. Our synthetic strategy has several advantages. First, the addition of the hydroxamic acid anchoring group is efficient and leads to greatly improved water tolerance and, thus, can be applied to a broad range of organic dyes bearing the cyanoacrylate anchoring group. Second, the synthetic procedure is readily scalable and maintains high yields. Third, the formation of the tetrahydropyran (THP)-protected hydroxylamine enables purification of the product prior to deprotection.

After isolation, MK-2HA dye was subsequently re-dissolved in toluene for sensitization of TiO_2 nanoporous films. However, preliminary results suggest that MK-2THP can undergo an *in situ* catalyzed deprotection at the surface of the TiO_2 substrate to form a dye monolayer. We believe that the hydroxylated surface of the TiO_2 substrate can act as a local acidic medium catalyzing the deprotection of MK-2THP which is followed by subsequent adsorption of the hydroxamate anchoring group to the substrate. Although additional experiments are underway to better characterize this process, the ability to perform the deprotection step *in situ* may render the process more appealing for practical application.

Extensive characterization of the MK-2HA and MK-2 dyes confirms that the anchoring group has minimal effects on the advantageous physicochemical properties of the dye itself. UV-visible spectra obtained in toluene (Fig. S1A, ESI†) confirm that the main peak of the MK-2HA is centered at 490 nm, which is essentially identical to the main peak of MK-2 (494 nm). The extinction coefficients of the MK-2 and MK-2HA are also essentially identical (Fig. S1, ESI†), when measured in either toluene or THF. Deprotonation of the MK-2 and MK-2HA dye in basic media (Fig. S1, ESI†) reveal that both dyes undergo comparable blue shifts of ~50 nm.

Quantitative determination of the optical and electrochemical parameters (Table 2) was performed with the ester- and THP-analogs of the MK-2 and MK-2HA dyes, respectively, because of their more ideal behavior (*cf.* ESI†) in comparison with the acid analogs. The fluorescence spectra (Fig. S2, ESI†) show that MK-2THP and MK-2E have nearly identical fluorescence peaks centered at 679 nm and 684 nm, respectively. The fluorescence lifetimes of the dyes in dichloromethane were found to have a bi-exponential behavior and the measured lifetimes (Table 2) are similar for the two dyes. The MK-2E had a major component of 665 ps (92%) and minor component of 1.45 ns (8%), while those for MK-2-THP were 712 ps (89%) and 1.30 ns (11%). The bi-exponential fluorescence decay has been observed previously in analogous dyes.[46,47] More importantly, these values are considerably larger than the sub-picosecond time scale of electron injection into TiO_2 as measured by THz spectroscopy (*cf.* Section 3.3).

Table 2 Physicochemical properties of the protected MK-2E and MK-2THP dyes

Dye	Absorption[a] (λ_{max}/nm)	Emission[a,b] (λ_{max}/nm)	E_{0-0} (eV)	τ_S[c] (ns)	E_{ox1}[d]	E_{ox2}[d] (*V vs.* NHE)	E_{ox}^{*}[e]
MK-2E	309, 384, 493	684	2.16	0.665 (92%) 1.45 (8%)	1.01	1.26	−1.15
MK-2THP	307, 384, 489	679	2.18	0.712 (89%) 1.30 (11%)	1.03	1.27	−1.15

[a] Experiment performed in dichloromethane solvent. [b] Excitation occurred at 459 nm at absorbance values below 0.08. [c] Excited using LED with peak emission at 459 nm. [d] Values for $E_{1/2}$. Electrochemistry performed in dichloromethane containing 100 mM $TBAPF_6$ electrolyte with ferrocene as internal reference. Oxidations were reversible. [e] Calculated $E_{ox1}-E_{0-0}$ using experimental data in dichloromethane solvent.

Electrochemical characterization of MK-2E and MK-2THP shows two reversible oxidation waves (Fig. S3, ESI†). The potentials for the first oxidation of MK-2THP and MK-2E were measured at 1.03 V and 1.01 V *vs.* NHE, respectively. Using the excited state energy of the dye and the measured potentials for oxidation, the excited state reduction potentials were calculated to be −1.15 V *vs.* NHE for both MK-2E and MK-2THP. Thus, the driving force for photo-induced IET into the conduction band of TiO_2 is identical.

3.2 Photoelectrochemical performance & impedance spectroscopy of MK-2 dye as a function of surface linker

The electrical properties of the devices fabricated with MK-2 and MK-2HA dyes were analyzed by *j–V* measurements. In the case of the novel MK-2HA dye, DSSCs were prepared with working electrodes immersed in the dye solution for periods of 16 and 24 h to explore the effects of adsorption time on device performance. The resulting *j–V* curves and accompanying photovoltaic parameters are summarized in Fig. S4 (ESI†) and Table 3, respectively. The performance of these organic dyes was compared with the N719 dye (Fig. S5, ESI†) because it is a well-studied benchmark for the performance of Ru-based sensitizers.

The cells based on MK-2HA undergoing 16 h of adsorption and those based on MK-2 evince essentially identical efficiencies of 6.5% and 6.6%, which are higher relative to analogously prepared devices with N719. In contrast, a 30% loss in device efficiency upon modification of the MK-2 dye with a phosphonic acid anchoring group to promote increased heat stability was recently reported.[48] Thus, our results demonstrate that the high performance of MK-2 dye is retained upon modification with the hydroxamate anchoring group. The hydroxamate anchored MK-2HA devices show an increase in the short-circuit current density (j_{sc}) by as much as 17% with respect to the commercial MK-2. The increased j_{sc} values measured in the MK-2HA cells likely arises from the increase in the dye loading achieved with the MK-2HA dye compared to the MK-2 dye (Table 3).

Our theoretical findings (*cf.* Section 3.4) reveal that the orientation of the hydroxamate linked dye with respect to the TiO_2 surface is favorable for higher packing densities and is consistent with the higher dye loading. However, the MK-2 and MK-2HA devices exhibit comparable efficiencies as a result of the larger fill factor (FF) observed in the MK-2 devices.

Table 3 Photovoltaic performance of DSSCs prepared with electrolyte A and sensitized with the N719, MK-2 and MK-2HA dyes obtained under simulated one-sun illumination

Dye	Adsorption time (h)	Dye loading (nmol cm^{-2})	j_{sc} (mA cm^{-2})	V_{oc} (V)	FF (%)	η (%)
N719	16	292.7[a]	19.6	0.69	46	6.3
MK-2	16	198.7[b]	16.7	0.66	60	6.6
MK-2HA	16	228.0[b]	19.6	0.68	49	6.5
MK-2HA	24	—	17.7	0.65	60	6.9

[a] The dye desorption was performed in a basic solution of 0.1 M NaOH in water for the ruthenium dye. [b] The dye desorption was performed in 10 μL of a 1 M tetrabutylammonium hydroxide solution dissolved into 15 mL of THF for organic dyes.

It is interesting to note that the j_{sc} value for the MK-2HA dye (16 h adsorption) is essentially identical to that of the N719 benchmark cell, even though dye loading of the latter is 28% higher. This is attributed to the nearly three-fold higher molar absorption coefficient of the MK-2HA dye (29 400 M^{-1} cm^{-1}) relative to that of the N719 dye (12 800 M^{-1} cm^{-1}).

The devices all have comparable V_{oc} values of roughly 0.67 ± 0.02 V. This is not surprising since the V_{oc} is determined by the difference of the Fermi level of electrons in the TiO_2 and the redox potential (E_{redox}) of the electrolyte ($qV_{oc} = E_{F,n} - E_{redox}$). The slight variation in the measured values can be attributed to the fact that in practice the V_{oc} depends on several factors including the energy mismatches between E_{redox} and HOMO levels of the dye, and between the conduction band E_c of the semiconductor and the LUMO of the dye.[49] A detailed investigation of the V_{oc} behavior was performed by means of impedance spectroscopy as described below.

In order to optimize the adsorption time of our modified organic dye, devices prepared with MK-2HA after 16 h and 24 h adsorption times were examined. The device prepared after a 24 h adsorption time yielded the highest overall efficiency among all of the devices of 6.9%. In previous reports, it was found that the coverage of MK-2 dye increases with increasing adsorption time; however, beyond 12 h the increase in coverage is accompanied by the corresponding formation of dye aggregates with diameters of up to 10 nm.[24,50] Accordingly, we observe a significant increase in the FF from 49% to 60%. The increase in the FF can be attributed to several plausible and previously observed mechanisms such as an increase in the coverage of the TiO_2, aggregation of the dye molecules at the interface, and re-organization of the structure of the dye monolayer with increasing adsorption time.[24,50] On the other hand, the j_{sc} decreases from 19.6 mA cm^{-2} to 17.7 mA cm^{-2} as the adsorption time is increased, which is also likely a result of dye aggregation on the TiO_2 surface. Previous work found that dye aggregation decreases the conversion of incident photons to charge carriers due to shorter excited state lifetimes and also increases electron recombination with the oxidized dye molecules.[9] In the present case, the improvement in the FF (22%) is more significant than the decline in the j_{sc} (11%), and leads to the best overall performance.

Electrochemical impedance spectroscopy (IS) was employed as an alternating current (AC) technique to further characterize the devices prepared with MK-2 analogs and N719 as a reference.[42,51] IS measurements are based on the electrical response of the DSSC, and are analyzed to provide insight into device parameters such as charge transport, recombination, carrier accumulation, and diffusion. Here, we focus on the recombination resistance (R_{rec}) and chemical capacitance (C_μ) extracted from fitting impedance spectra measured under simulated one-sun illumination over a range of applied voltages.[49,51] These parameters are presented as a function of Fermi level voltage (V_F) in Fig. 1. When comparing different devices, it is important to account for the voltage drop due to series resistance (R_{series}) arising from the FTO conducting glass, electrolyte diffusion, and platinum counter electrode. Thus, we can obtain the Fermi level voltage V_F, as the difference

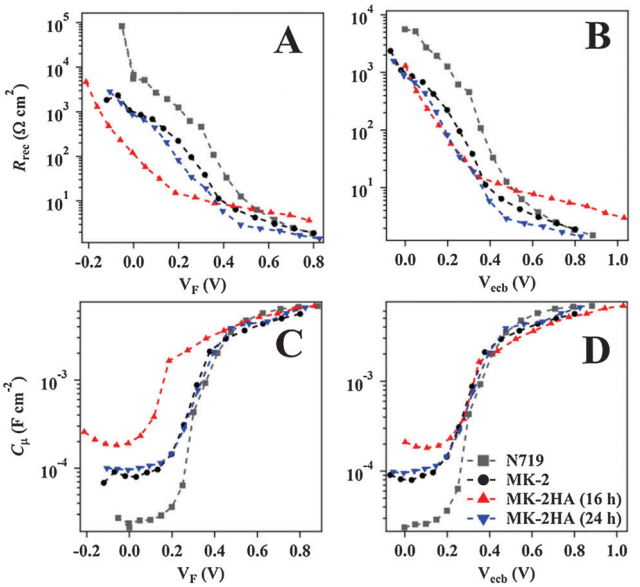

Fig. 1 Recombination resistance (R_{rec}, A & B) and chemical capacitance (C_μ, C & D) with respect to the Fermi level voltage (V_F, A & C) and with respect to the equivalent common conduction band voltage (V_{ecb}, B & D) for solar cells prepared with electrolyte A and sensitized with N719, MK-2 and MK-2HA after 16 h and 24 h of adsorption.

between the applied voltage (V_{app}) and the voltage drop at the total series resistance *i.e.*, $V_F = V_{app} - V_{series}$, where V_{series} is defined in eqn (1).

$$V_{series} = \left(\frac{j}{j_{sc} - j}\right)\int_{j_{sc}}^{j} R_{series}\,dj \quad (1)$$

The dependence of R_{rec} and C_μ on V_F is shown in Fig. 1A and C, respectively. In both cases, the R_{rec} and C_μ exhibit an exponential dependence at biases between 0.2 and 0.4 V according to eqn (2) and (3), respectively,

$$R_{rec} = R_0 e^{(-q\beta V_F/k_B T)} \quad (2)$$

$$C_\mu = C_0 e^{(q\alpha V_F/k_B T)} \quad (3)$$

where C_0 and R_0 are constants, q is the magnitude of the electron charge, α is the exponential electron trap distribution parameter, β is the electron transfer coefficient from TiO_2 to the electrolyte ($\beta < 1$), k_B is Boltzmann's constant, and T is the temperature (K). At biases outside of the 0.2–0.4 V range, the R_{rec} and C_μ are essentially independent of the voltage.

The chemical capacitance C_μ is typically employed to estimate the position of conduction band edge of TiO_2 (E_{cb}).[51] For the purpose of comparing different devices, we use the exponentially rising or falling region, rather than the flat region at higher voltages, which is associated with partial pinning of the Fermi level. It is observed that C_μ at about 0.3 V is essentially identical for all of the devices, except the MK-2HA (16 h) cell. The shift in the band may attributed to the adsorption time; however, further experiments that are beyond the scope of this report are necessary to determine the origin of this shift.

In order to evaluate recombination rates, it is important to shift the recombination resistance by the same amount that the band moves (ΔE_{cb}).[52] Taking into account that the N719, MK-2 and MK-2HA (24 h) devices have a similar TiO_2 conduction band position, the ΔE_{cb} value was calculated for the MK-2HA (16 h) and was determined to be +163 mV. The R_{rec} and C_μ can be replotted with respect to the equivalent common conduction band voltage (V_{ecb}) in Fig. 1B and D, respectively, taking into account the definition of the V_{ecb} as $V_F - \Delta E_{cb}/q$.[52] It is now observed that the MK-2 and the MK-2HA (16 h and 24 h) have nearly the same R_{rec} values at low voltages (Fig. 1B), indicating that the charge recombination rate in these organic dyes is independent of adsorption time (16 h or 24 h). Additionally, the lower charge recombination rate (*i.e.* higher R_{rec}) observed in Fig. 1B for the N719 device with respect to the other DSSCs is reflected in the highest V_{oc} value shown in Table 3.

3.3 Injection and recombination dynamics of MK-2 and MK-2HA sensitized films

The recombination and injection dynamics of TiO_2 films sensitized with the MK-2 and MK-2HA dyes were studied by means of transient absorption (TA) spectroscopy and time-resolved THz spectroscopy (TRTS), respectively. TA spectroscopy was employed to observe the decay of the charge-separated state resulting from recombination of the oxidized dye with conduction band electrons following electron injection. The resulting TA profiles (Fig. 2A) demonstrate that the recombination rate is measurably slower in the MK-2HA (16 h) sensitized film than that of the MK-2 sensitized film. To quantitatively determine the recombination kinetics, the lifetimes of the charge-separated states were determined from the profiles (*cf.* ESI†) utilizing methods previously described in the literature.[53] The lifetime of the charge-separated state in MK-2HA was determined to be 82 μs, which was nearly 3.5-fold higher than the corresponding value of 24 μs for the MK-2 dye. This result confirms that the rate of recombination is slower in the MK-2HA than MK-2 and is consistent with the higher measured R_{rec} in the MK-2HA dye relative to MK-2.

Electron injection dynamics were studied by using TRTS. In TRTS, the dye-sensitized TiO_2 film is illuminated with a 400 nm pump beam leading to photoinduced electron injection. The electron injection rate and efficiency is measured by a THz probe beam, which is affected by mobile electrons in the conduction band of TiO_2. The TRTS results for MK-2, MK-2HA and N719 bound to TiO_2 nanoparticles are shown in Fig. 2B. It is apparent in the inset of Fig. 2B that electron injection for each of the sensitizers is completed within the ~300 fs response time of the instrument. Interestingly, the MK-2 and MK-2HA organic sensitizers exhibit more efficient electron injection than N719, and this provides further evidence that the MK-2 organic dyes outperform the Ru-based N719 dye. Amongst the organic sensitizers, the injection efficiency of MK-2 is measurably higher than that of MK-2HA. It is important to note that the differences in injection efficiency cannot be attributed to differences in absorption efficiency because both samples absorb nearly all of the light at 400 nm and have similar

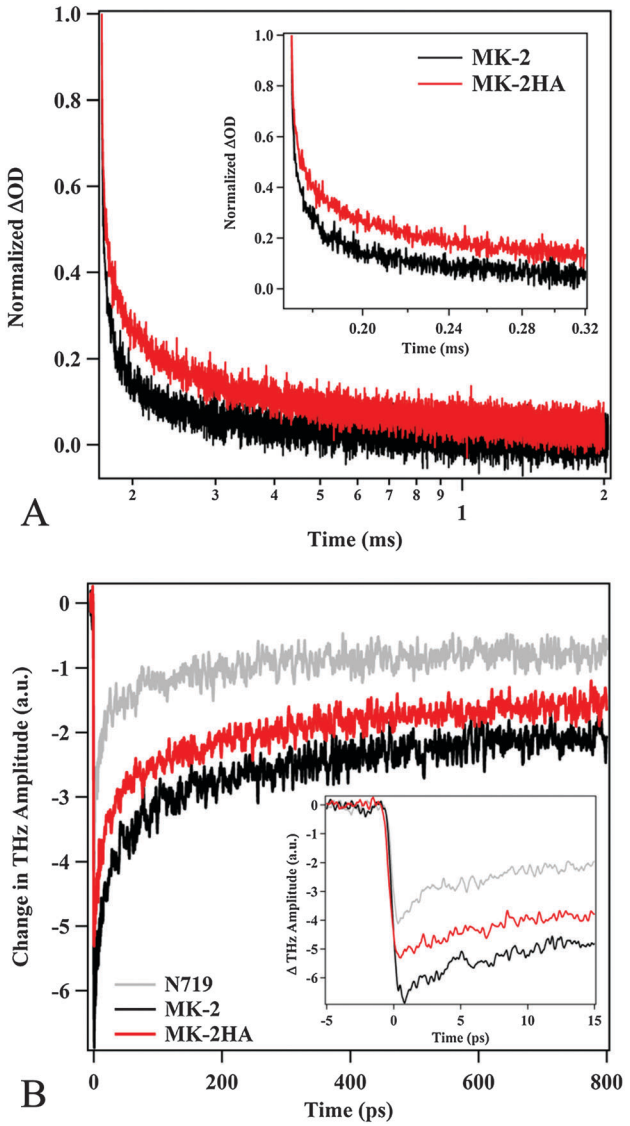

Fig. 2 Transient absorption traces (A) measured at 800 nm for the decay of the charge-separated state after photoinduced electron injection in films sensitized with MK-2 and MK-2HA dyes. Time-resolved THz results (B) show the relative electron injection efficiency of MK-2, MK-2HA and N719 sensitized films following photoexcitation at 400 nm. The insets highlight the first 320 μs and first 15 ps after photoinduced electron injection, respectively.

absorption coefficients (Fig. S1, ESI†). Therefore, these results suggest that the MK-2HA has a lower overall injection efficiency, which is consistent with the time-dependent IET simulations presented in the next section. Finally, the recovery of the THz signal shown in Fig. 1B can be attributed to electron trapping (femtosecond to tens of picosecond timescales),[54,55] rather than recombination, which was measured to occur on a timescale of ~20–80 μs.

It has been recently demonstrated in the case of analogous coumarin dyes that recombination of injected electrons with both the oxidized dye and the redox couple in the electrolyte solution contribute to a significant limitation of overall performance in functioning devices.[56] Thus, optimization of the dye–semiconductor interface to promote slower rates of recombination even at the expense of reduced electron injection efficiency has led to significantly improvements in overall device performance.[57–59] Collectively, our injection and recombination results suggest that the hydroxamate-modified dye promotes slower rates of recombination and higher measured recombination resistances. However, the gains in recombination are balanced by a corresponding decrease in the injection efficiency. Thus, it is not surprising that the MK-2 and MK-2HA dyes maintain comparable DSSC efficiencies.

3.4 Computational results

To complement our experimental characterization of the injection and recombination dynamics of the MK-2 dyes as a function of the anchoring group, we have investigated the IET time-scales for the MK-2 and MK-2HA dyes using time-dependent IET simulations. The details of our computational methods including the geometric optimization of the dyes and the IET simulations are described in the ESI.†[31,60] Initially, the structures of the frontier orbitals of the MK-2 dye with carboxylate and hydroxamate anchoring groups were obtained by performing geometry optimizations at the density functional level of theory. These calculations show that the shape and electron density distribution of the HOMO and LUMO frontier orbitals (Fig. S8, ESI†) are not significantly affected by the introduction of the hydroxamic acid moiety. In addition, the HOMO–LUMO gap is also essentially unaffected by the anchoring group, with both dyes maintaining a gap of ~2.1 eV. The UV-visible spectra of MK-2 and MK-2HA were calculated utilizing time-dependent DFT (TDDFT) calculations in vacuum. The resulting spectra depicted in Fig. S9A (ESI†) show two broad bands, consistent with the experimentally measured spectra (Fig. S1, ESI†). Although the peak positions obtained in vacuum are red-shifted in comparison with the experimental spectra, the relative intensities and positions of both peaks are well reproduced. The orientation and strength of the transition dipole moments for the first excitation are essentially identical for both original (Fig. S9B, ESI†) and modified (Fig. S9C, ESI†) dyes. To simulate the structure of the dye–semiconductor interface, the MK-2 and MK-2HA dyes were anchored to an anatase TiO_2(101) surface utilizing the optimized anchoring configurations calculated from benzoic acid and phenyl-hydroxamic acid.[60] In the case of the MK-2 system, the optimized geometry of the dye molecule is tilted with respect to the surface normal vector, which is depicted in Fig. 3B. In contrast, the tilt-angle for the MK-2HA dye is smaller (Fig. 3C). Based on prior results, differences in the tilt-angle of surface adsorbed dyes can modify the IET dynamics as a result of factors such as strain and the relative orientation of the transition dipole moment respect to the TiO_2 surface.[60,61] Herein, the slight difference in the orientation of the MK-2 and MK-2HA molecules may lead to their distinctive IET properties, although additional work beyond the scope of this report is necessary to fully explore this issue.

Time-dependent IET simulations of the full anatase TiO_2(101) sensitized surface slabs were performed to compute the IET time scales for both the MK-2 and MK-2HA dyes.[60] The calculated survival probability, which represents the

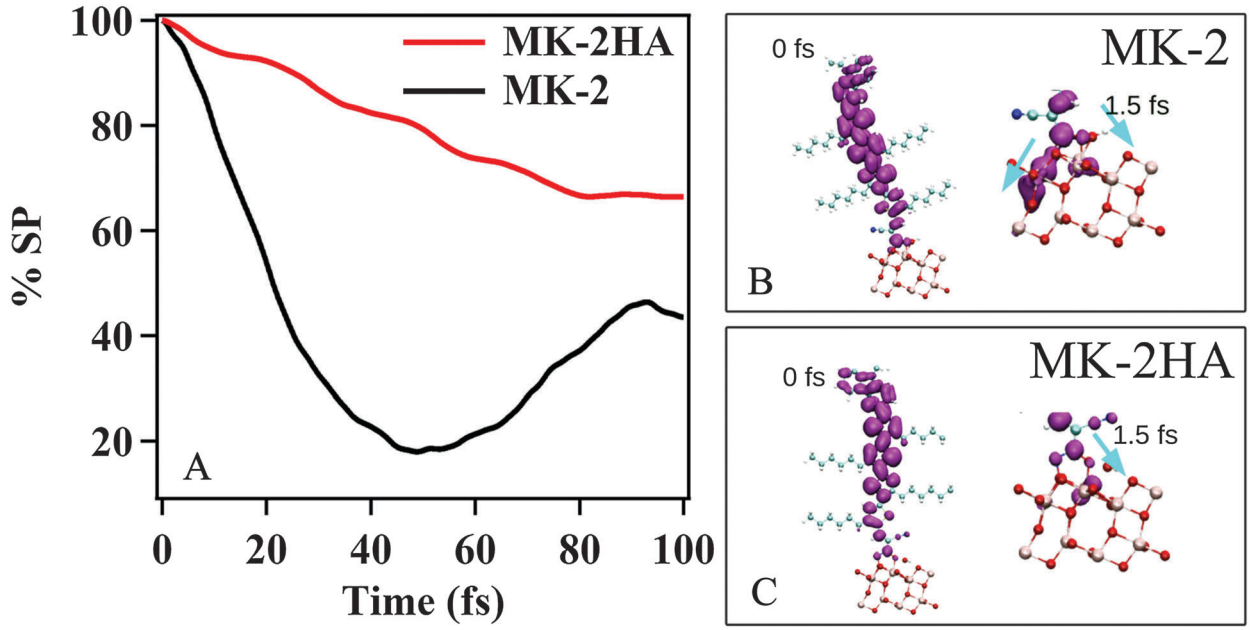

Fig. 3 Survival probability (A) as a function of time for MK-2 and MK-2HA. Schematic representations of the anchoring geometries and snapshots of the electron density calculated at 0 fs (left) and 1.5 fs (right) are shown for the MK-2 (B) and MK-2HA (C) dyes. In this depiction, the Ti, C, N, O, S and H atoms are represented by pink, light blue, blue, red, yellow and white spheres, respectively and blue arrows indicate charge-transfer pathways from the dye to the semiconductor.

relative probability for the electron to remain on the photo-excited adsorbate (Fig. 3A) suggest that both dyes exhibit ultrafast, sub-picosecond IET. However, the unmodified MK-2 dye shows a considerably faster rate of IET, and at 50 fs nearly 80% of the electron density is injected. In contrast, only about 20% is injected at 50 fs for the case of MK-2HA. The slower injection rate of the MK-2HA dye is consistent with the measured injection efficiency results experimentally determined by TRTS measurements.

In addition to calculating the IET dynamics, we also include a representation of the initial electronic charge distribution for both systems (Fig. 3B and C), in order to rationalize the difference in IET rates of the two dyes. Differences in the calculated injection rate could arise from differences in the coupling of the initial state with the anatase (101) surface. The electron dynamics simulation shows that two-electron density pathways are available for the case of MK-2 while MK-2HA shows only one.

Collectively, the results in Sections 3.3 and 3.4 suggest that the photoelectrochemical performance arises from a balance between the rates of recombination and electron injection efficiency in the MK-2 and MK-2HA dyes. We find that MK-2 has a larger number of charge-transfer pathways leading to increased injection efficiency and faster recombination, whereas the MK-2HA establishes only one charge-transfer pathway and has correspondingly lower injection efficiency and slower recombination. Thus, it is evident that these competing trends balance in both cases, and leads to essentially identical overall performance when these dyes are employed in DSSC devices (*cf.* Section 3.2). This interesting finding highlights the importance of the anchoring group not only in terms of long-term durability but also in terms of tailoring the IET dynamics of dye molecules.

3.5 Water stability and durability of sensitized films as a function of anchoring group

In this section, we demonstrate that the modification of the cyanoacrylate acceptor group with a hydroxamate surface anchoring group dramatically improves the water tolerance of the dye–semiconductor interface. The water stability of the modified MK-2HA dye was compared to the as-received, commercial MK-2 dye by immersing sensitized films into solutions of DMF containing 0.1, 0.5 and 1 vol% water. DMF was chosen (*cf.* ESI†) as the desorption solvent because of its unique ability to co-solubilize both water and the MK-2 dyes. As a control experiment, the sensitized films were also immersed into anhydrous DMF containing only trace quantities ($<0.005\%$) of water.

The measured desorption curves (Fig. 4A–C) reveal that the MK-2HA dye desorbs at a considerably slower rate than the MK-2 dye over the course of each experiment. Fig. 4D provides a comparison of the percentage of dye retained on the TiO_2 surface after a period of four hours when immersed in DMF with varying water content. The results conclusively demonstrate that 30–50% more MK-2HA than commercial MK-2 remains on the surface under each condition. Desorption curves were fit assuming a first-order desorption model (*cf.* Fig. S10, ESI†), in order to determine the relevant kinetic parameters summarized in Table S1 (ESI†). Not surprisingly, the measured desorption rate constants are 30–60% lower in the case of MK-2HA dye. We also demonstrate below that the MK-2HA films retain larger percentages of the dye monolayer that most efficiently contributes to IET under each of the desorption conditions. These results

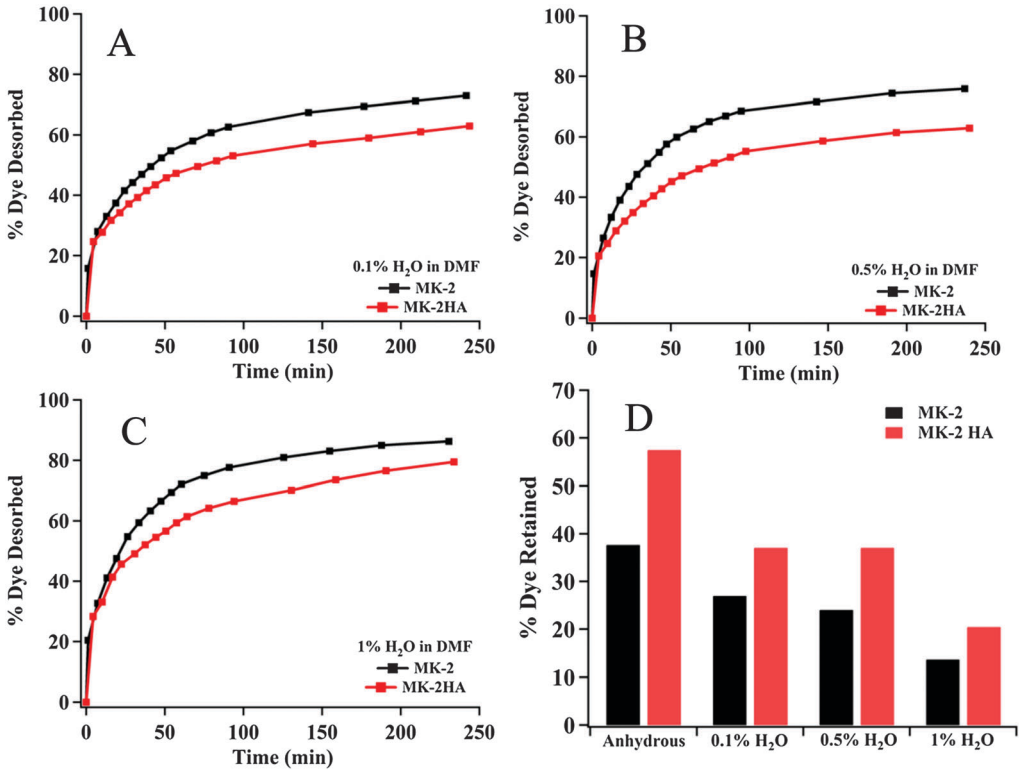

Fig. 4 Desorption curves (A–C) of the MK-2HA and MK-2 dyes from sensitized TiO_2 films immersed into DMF containing 0.1%, 0.5%, and 1% water, respectively. The percentage of dye retained on the electrode surface (D) is shown after an immersion time of four hours in DMF solutions.

confirm that tailoring the anchoring group of the MK-2 dye results in considerable improvements in the water stability of the dye–semiconductor linkage. The enhanced water tolerance can be attributed to several factors including: (i) a higher pK_a and (ii) a less strained chelate bite angle in hydroxamic acids compared with carboxylic acid analogs.[31,32]

Our findings suggest that water promotes desorption by hydrolyzing the carboxylate and hydroxamate linkages to the TiO_2 surface, as opposed to degrading the dye backbone itself.[27] First, the UV-visible spectrum obtained from the solution of desorbed MK-2 dye in 1% H_2O in DMF was essentially identical to the spectrum obtained from the as-received dye in the same solution (Fig. S11, ESI†). Similar results were noted with the MK-2HA dye, suggesting that the structure and optical properties of the dyes remain unchanged upon desorption. Second, we demonstrate that the desorption process for both MK-2 and MK-2HA reaches equilibrium, since simultaneous immersion of a dye-sensitized and a pristine TiO_2 film result in essentially equivalent dye loading on both films. In all cases, the fraction of dye remaining on the electrode is measurably higher in the case of the MK-2HA films, indicating that the hydroxamate anchoring group is less susceptible to hydrolysis and desorption.

To examine the effect of desorption on electron injection and recombination, we have measured the IET dynamics of TiO_2 films sensitized with the MK-2 and MK-2HA dyes before and after desorption. Fig. 5 compares the electron injection efficiency for the MK-2 and MK-2HA sensitized films before and after immersion in a solution of 1% water in DMF.

Surprisingly, the MK-2HA film shows essentially no change in the electron injection efficiency upon exposure to the desorption solution (Fig. 5B). On the other hand, the initial injection efficiency decreased by nearly 65% in the MK-2 film (Fig. 5A), highlighting the sensitivity of the dye–semiconductor interface toward water.

The effect of dye desorption on the lifetimes of the charge-separated state was examined by TA spectroscopy. Fig. 5C reveals that for both the MK-2HA and MK-2 dye the lifetime of the charge-separated state increases with increasing immersion time in the DMF–water solution. In the case of the MK-2HA, the lifetime of the as-prepared film (54 μs) is increased nearly 3-fold to 145 μs. Since there is no loss in overall injection efficiency upon desorption of the dye, the soaking and desorption represents a potentially effective treatment for improving the recombination dynamics of the sensitized film itself. The increased lifetime of the charge-separated state in both cases can be attributed to the removal of dye aggregates from the surface, among other plausible mechanisms.[24] For example, these results are in agreement with recent results by O'Regan *et al.*[62] suggesting that the exposure of the TiO_2 surface to various treatments particularly after dye desorption can greatly influence the recombination of injected electrons with the redox couple in the electrolyte solution.

To evaluate the dyes in an environment more closely resembling that of a functioning DSSC device, we also examine the effect of the concentration of water on the lifetime of the charge separated state. The results (Fig. 5D) show that the MK-2HA exhibits longer

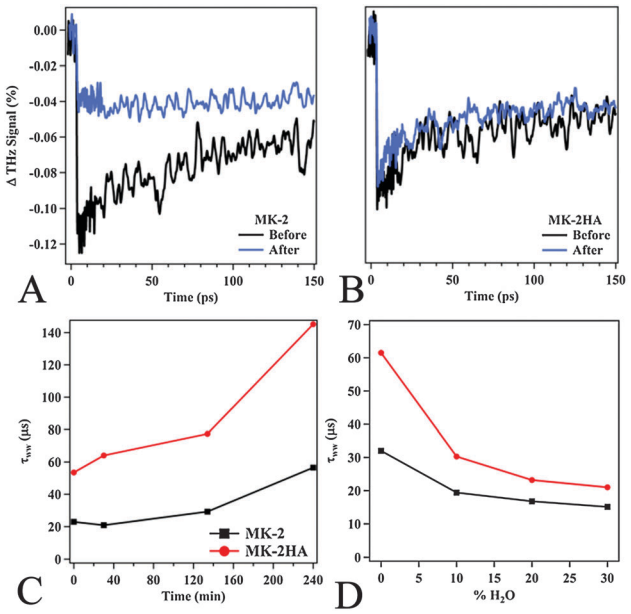

Fig. 5 Time-resolved THz measurements highlighting the relative electron injection efficiency of MK-2 (A) and MK-2HA (B) sensitized films before and after immersion in a solution of 1% water in DMF for a period of four hours. The trend in the lifetime of the charge-separated state (τ_{ww}) as a function of soaking time (C) in a 1 vol% solution of water in DMF. The lifetime of the charge-separated state as a function of the percentage of water present (D) in the acetonitrile–water mixture used during the TA experiment.

lifetimes when up to 30% water is purposefully added to the acetonitrile solvent. In a broader sense, the spectroscopic results confirm that the MK-2HA maintains better performance than the commercial dye in the presence of water, which is a strong indication that incorporation of hydroxamic acid in the dye design can lead to better water tolerance in actual devices.

3.6 Long-term water stability and durability of DSSC devices as a function of anchoring group

The infiltration of water into the electrolyte of DSSCs has been of particular concern in the context of long-term stability, since the covalent bonds between the dye and TiO_2 surface can be hydrolyzed in the presence of water.[10] On the basis of the promising water stability of the hydroxamate modified MK-2 dye presented in Section 3.5, we investigate the water stability under operating cell conditions of MK-2HA dye in comparison with the commercially available dye and the N719 benchmark. DSSC devices were prepared as described in the ESI† with electrolytes containing increasing amounts of water and the performance of these devices was measured over a period of 200 h. For these studies, electrolyte formulation B was employed in order to co-solubilize the TBP, iodine and water. The significant difference in the composition of electrolyte B from electrolyte A, which is optimized for the MK-2 dye, renders it impossible to directly compare the performance of devices in this section with those in Section 3.2.

The external quantum efficiencies (EQEs) shown in Fig. 6 highlight the effect of water on charge generation and collection of the MK-2 and MK-2HA-based solar cells with the concentration of water carefully controlled in the electrolyte. It is noteworthy that the EQE increases in the MK-2HA DSSCs (Fig. 6B) as the water content is increased from trace levels in the control cell to the cells possessing 10 and 20% water. This surprising result shows that 10% water can measurably increase the number of photogenerated electrons per photon of a given wavelength (by nearly 20% at 500 nm, for example). In contrast, the devices sensitized with commercial MK-2 undergo ~20% decline in the EQE signal at 500 nm, which is consistent with the corresponding decrease in the measured j_{sc} for these devices (Fig. 7).

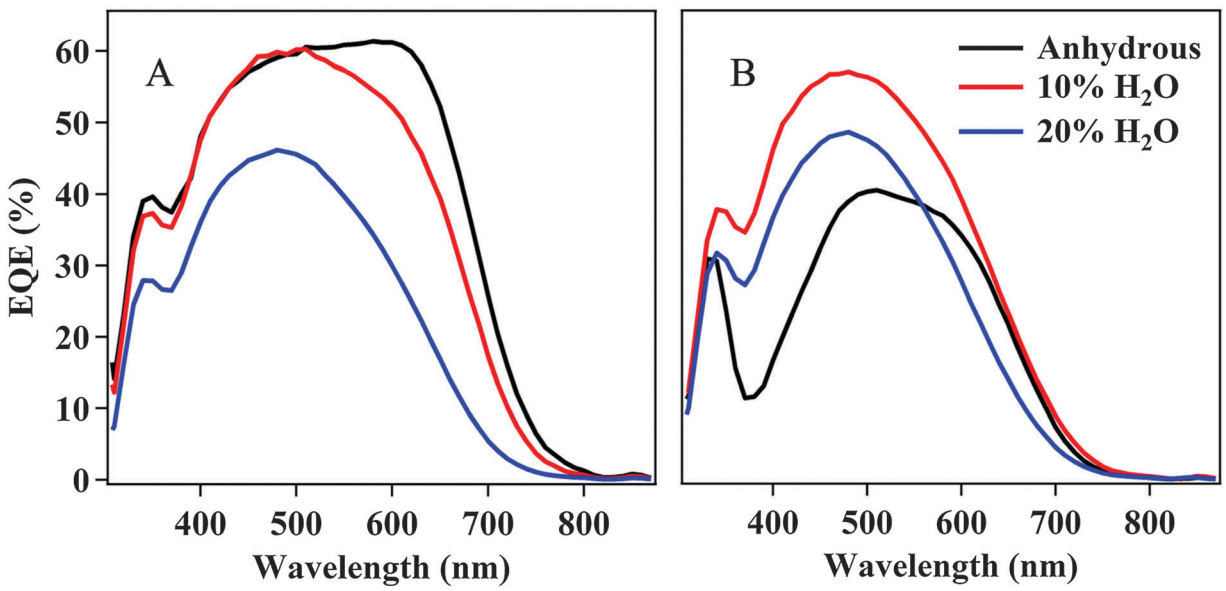

Fig. 6 External quantum efficiency (EQE) spectra for the MK-2 (A) and MK-2HA (B) DSSCs prepared with 0%, 10% and 20% water incorporated into electrolyte B.

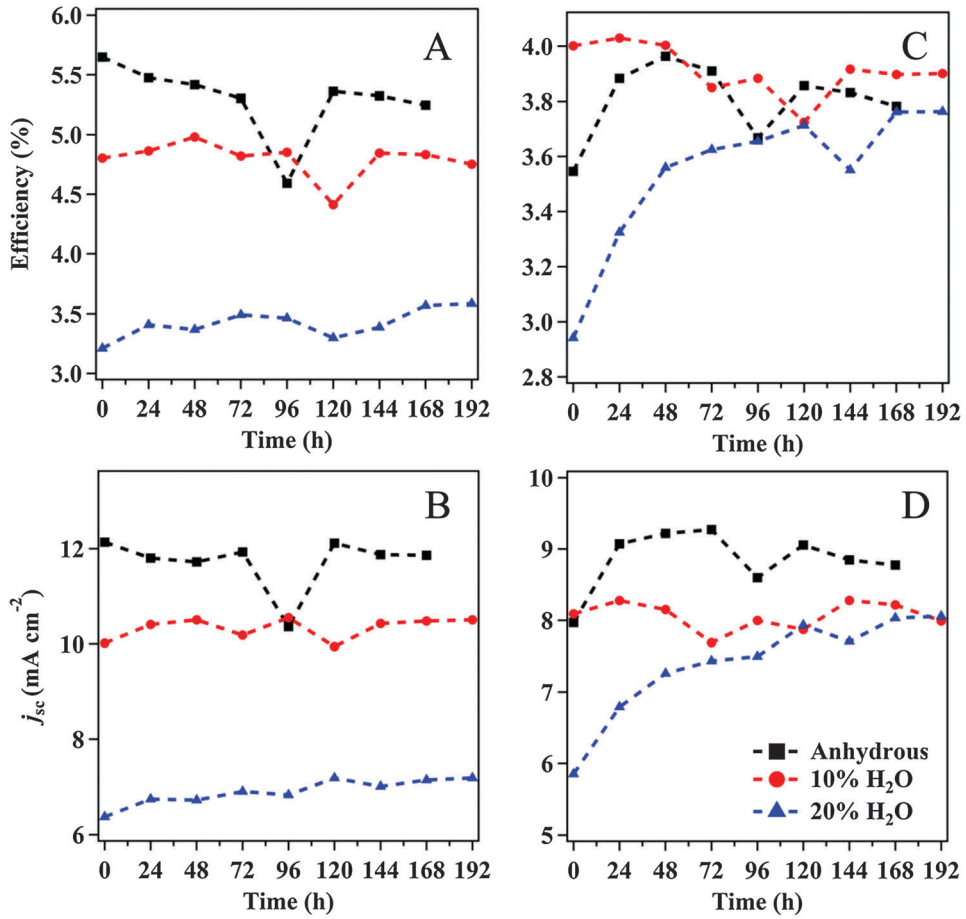

Fig. 7 Time evolution of the efficiency (A & C) and j_{sc} (B & D) photovoltaic parameters under one-sun simulated illumination for the MK-2 (A & B) and MK-2HA (C & D) devices containing specified amounts of water in electrolyte B.

The photovoltaic results collected over the eight-day durability test of the MK-2 and MK-2HA devices are summarized in Fig. 7 and Fig. S12 (ESI†). The devices were aged in the dark at ambient conditions and photovoltaic measurements were obtained periodically under one-sun irradiation (AM1.5G). Each point in the graphs represents an average of three devices. Fig. S13 and S14 (ESI†) include the same graphs with error bars, which are omitted in Fig. 7 for clarity. On the basis of a statistical analysis (*cf.* ESI†), we consider the overall trends in the solar cell parameters as a function of time and not deviations of single data points since the sometimes large point-to-point variations are associated with inherent noise in the experiment.

In the case of the commercial MK-2 dye (Fig. 7A), the results conclusively demonstrate that the devices with 10% and 20% water in the electrolyte have decreased efficiency by 15% and 50% compared to the anhydrous control. Reduced performance is primarily associated with the 50% decrease in the j_{sc} value (Fig. 7B) from 12 mA cm^{-2} in the control cells to 6 mA cm^{-2} in the cells with 20% water. The remarkable decline in the j_{sc} values is consistent with the decreased IET efficiency and lower EQE upon exposure of MK-2 films to water. Fig. S12A (ESI†) also reveals that the addition of water results in lower V_{oc} values in the cells containing water at the start of the test. Over the course of the test, the V_{oc} of the cells with 10% and 20% water in the electrolyte are stable at 737 mV and 675 mV, respectively. However, the anhydrous cell undergoes a 6% decrease from 740 mV to 690 mV suggesting that the addition of water may serve to stabilize the V_{oc} in the devices sensitized with commercial MK-2. In terms of the FF results shown in Fig. S12B (ESI†), the anhydrous and 10% H_2O electrolytes possess identical values of approximately 65%, while the FF for the 20% cell is ~75%. Although it is difficult to rationalize the trend in the FF, the increase may be associated with a lower series resistance as water is added to the cells.[33]

In stark contrast with the commercial MK-2 devices, the efficiency of the hydroxamate modified MK-2HA cells is significantly less sensitive to the presence of water in the electrolyte. At the conclusion of the test, there is no significant difference in the efficiencies (<5%) measured from the cells containing water in the electrolyte and the anhydrous cell (Fig. 7C). In this case, the increase in performance is correlated with the FF and V_{oc} parameters, which are both increased by the addition of water (Fig. S12C and D, ESI†). On the other hand, there is no significant difference between the measured j_{sc} values (Fig. 7D) by the conclusion of the test among the three types of cells. An interesting trend is noted in the evolution of the efficiency and

j_{sc} and in the case of the cell prepared with 20% water. Specifically, these parameters were found to increase by 30% and 25%, respectively, over the course of the first 96 h of the test. While it is difficult to determine the origin of this trend, our desorption and injection efficiency results suggest that the water content in the electrolyte may serve to accelerate the desorption of aggregates leading to more favorable IET dynamics.

4. Conclusions

In this article, a straightforward and efficient synthetic protocol is employed to modify the existing cyanoacrylic acid moiety of the state-of-the-art MK-2 organic dye with a highly water stable hydroxamic acid anchoring group. Extensive characterization of the resulting MK-2HA dye confirms that the hydroxamate anchoring group modification does not significantly affect the favorable optoelectronic properties of the dye. In fact, DSSC devices prepared with the MK-2HA dye evince the highest overall efficiency (6.9%), when compared with devices prepared with the commercial MK-2 dye and N719 dyes. Results from IS and TA spectroscopy suggest that the hydroxamate anchoring group yields a higher recombination resistance and accordingly slower recombination rates of the injected electron leading to the observed increase in device efficiency.

We have also extensively studied the water stability of the dye–semiconductor interface as a function of anchoring group. Desorption experiments conducted in the presence of water confirm that the covalent interaction between the MK-2HA dye and TiO_2 is significantly more stable toward desorption than the commercial MK-2 dye. Given the promising results from the desorption study, the water stability of the MK-2HA and MK-2 dyes were studied within working DSSC devices with known quantities of water incorporated into the electrolyte. The results demonstrate that the hydroxamate anchoring group leads to essentially no loss in device efficiency over the course of the eight days, which is in stark contrast with the decline in efficiency of up to 50% for cells prepared with the commercial dye. Collectively, these results demonstrate the modification of organic dyes with hydroxamate anchoring groups utilizing the simple synthetic protocol described herein can lead to significant increases in long-term device durability and increased overall device performance.

Acknowledgements

This work was supported by the generous donation made from the TomKat Charitable Trust. Part of this work was also supported by the facilities and staff of the Yale University Faculty of Arts and Sciences High Performance Computing Center and by the National Science Foundation under grant #CNS 08-21132 that partially funded acquisition of the facilities. We acknowledge support by Generalitat Valenciana project ISIC/2012/008. Additional funding for THz experiments came from the Office of Basic Energy Sciences of the U.S. Department of Energy (DE-FG02-07ER15909).

References

1 M. S. Prévot and K. Sivula, *J. Phys. Chem. C*, 2013, **117**, 17879–17893.
2 J. R. Swierk and T. E. Mallouk, *Chem. Soc. Rev.*, 2013, **42**, 2357–2387.
3 L. Duan, L. Tong, Y. Xu and L. Sun, *Energy Environ. Sci.*, 2011, **4**, 3296–3313.
4 H. S. Jung and J.-K. Lee, *J. Phys. Chem. Lett.*, 2013, **4**, 1682–1693.
5 P. K. Nayak, J. Bisquert and D. Cahen, *Adv. Mater.*, 2011, **23**, 2870–2876.
6 B. O'Regan and M. Grätzel, *Nature*, 1991, **353**, 737–740.
7 M. K. Nazeeruddin, A. Kay, I. Rodicio, R. Humphry-Baker, E. Mueller, P. Liska, N. Vlachopoulos and M. Grätzel, *J. Am. Chem. Soc.*, 1993, **115**, 6382–6390.
8 N. Tetreault and M. Grätzel, *Energy Environ. Sci.*, 2012, **5**, 8506–8516.
9 A. Hagfeldt, G. Boschloo, L. Sun, L. Kloo and H. Pettersson, *Chem. Rev.*, 2010, **110**, 6595–6663.
10 R. Harikisun and H. Desilvestro, *Sol. Energy*, 2011, **85**, 1179–1188.
11 L. Wang, X. Fang and Z. Zhang, *Renewable Sustainable Energy Rev.*, 2010, **14**, 3178–3184.
12 J. Xia and S. Yanagida, *Sol. Energy*, 2011, **85**, 3143–3159.
13 Q. Zhang, E. Uchaker, S. L. Candelaria and G. Cao, *Chem. Soc. Rev.*, 2013, **42**, 3127–3171.
14 I. Martini, J. H. Hodak and G. V. Hartland, *J. Phys. Chem. B*, 1999, **103**, 9104–9111.
15 R. L. Milot, G. F. Moore, R. H. Crabtree, G. W. Brudvig and C. A. Schmuttenmaer, *J. Phys. Chem. C*, 2013, **117**, 21662–21670.
16 N. Martsinovich, F. Ambrosio and A. Troisi, *Phys. Chem. Chem. Phys.*, 2012, **14**, 16668–16676.
17 A. Reynal and E. Palomares, *Eur. J. Inorg. Chem.*, 2011, 4509–4526.
18 M. K. Nazeeruddin, F. De Angelis, S. Fantacci, A. Selloni, G. Viscardi, P. Liska, S. Ito, B. Takeru and M. Grätzel, *J. Am. Chem. Soc.*, 2005, **127**, 16835–16847.
19 S. Ito, S. M. Zakeeruddin, R. Humphry-Baker, P. Liska, R. Charvet, P. Comte, M. K. Nazeeruddin, P. Péchy, M. Takata, H. Miura, S. Uchida and M. Grätzel, *Adv. Mater.*, 2006, **18**, 1202–1205.
20 B.-G. Kim, K. Chung and J. Kim, *Chem. – Eur. J.*, 2013, **19**, 5220–5230.
21 S. Kim, J. K. Lee, S. O. Kang, J. Ko, J. H. Yum, S. Fantacci, F. De Angelis, D. Di Censo, M. K. Nazeeruddin and M. Grätzel, *J. Am. Chem. Soc.*, 2006, **128**, 16701–16707.
22 Z. S. Wang, Y. Cui, K. Hara, Y. Dan-oh, C. Kasada and A. Shinpo, *Adv. Mater.*, 2007, **19**, 1138–1141.
23 N. Koumura, Z.-S. Wang, S. Mori, M. Miyashita, E. Suzuki and K. Hara, *J. Am. Chem. Soc.*, 2006, **128**, 14256–14257.
24 Z.-S. Wang, N. Koumura, Y. Cui, M. Takahashi, H. Sekiguchi, A. Mori, T. Kubo, A. Furube and K. Hara, *Chem. Mater.*, 2008, **20**, 3993–4003.
25 X.-H. Zhang, J. Ogawa, K. Sunahara, Y. Cui, Y. Uemura, T. Miyasaka, A. Furube, N. Koumura, K. Hara and S. Mori, *J. Phys. Chem. C*, 2013, **117**, 2024–2031.

26 Y. Wu and W. Zhu, *Chem. Soc. Rev.*, 2013, **42**, 2039–2058.
27 C. Chen, X. Yang, M. Cheng, F. Zhang and L. Sun, *ChemSusChem*, 2013, **6**, 1270–1275.
28 S. G. Abuabara, C. W. Cady, J. B. Baxter, C. A. Schmuttenmaer, R. H. Crabtree, G. W. Brudvig and V. S. Batista, *J. Phys. Chem. C*, 2007, **111**, 11982–11990.
29 W. R. McNamara, R. C. Snoeberger, G. Li, J. M. Schleicher, C. W. Cady, M. Poyatos, C. A. Schmuttenmaer, R. H. Crabtree, G. W. Brudvig and V. S. Batista, *J. Am. Chem. Soc.*, 2008, **130**, 14329–14338.
30 S. G. Abuabara, L. G. C. Rego and V. S. Batista, *J. Am. Chem. Soc.*, 2005, **127**, 18234–18242.
31 W. R. McNamara, R. C. Snoeberger, G. Li, C. Richter, L. J. Allen, R. L. Milot, C. A. Schmuttenmaer, R. H. Crabtree, G. W. Brudvig and V. S. Batista, *Energy Environ. Sci.*, 2009, **2**, 1173–1175.
32 W. R. McNamara, R. L. Milot, H.-e. Song, R. C. Snoeberger III, V. S. Batista, C. A. Schmuttenmaer, G. W. Brudvig and R. H. Crabtree, *Energy Environ. Sci.*, 2010, **3**, 917–923.
33 K. Zhu, S.-R. Jang and A. J. Frank, *Energy Environ. Sci.*, 2012, **5**, 9492–9495.
34 C. Law, O. Moudam, S. Villarroya-Lidon and B. O'Regan, *J. Mater. Chem.*, 2012, **22**, 23387–23394.
35 B. J. Brennan, M. J. Llansola Portoles, P. A. Liddell, T. A. Moore, A. L. Moore and D. Gust, *Phys. Chem. Chem. Phys.*, 2013, **15**, 16605–16614.
36 B. J. Brennan, A. E. Keirstead, P. A. Liddell, S. A. Vail, T. A. Moore, A. L. Moore and D. Gust, *Nanotechnology*, 2009, **20**, 505203.
37 L. A. Martini, G. F. Moore, R. L. Milot, L. Z. Cai, S. W. Sheehan, C. A. Schmuttenmaer, G. W. Brudvig and R. H. Crabtree, *J. Phys. Chem. C*, 2013, **117**, 14526–14533.
38 T. P. Brewster, S. J. Konezny, S. W. Sheehan, L. A. Martini, C. A. Schmuttenmaer, V. S. Batista and R. H. Crabtree, *Inorg. Chem.*, 2013, **52**, 6752–6764.
39 J. Chen, R. H. Crabtree, 2013, Unpublished Data.
40 A. Mishra, M. K. R. Fischer and P. Bäuerle, *Angew. Chem., Int. Ed.*, 2009, **48**, 2474–2499.
41 E. M. Barea, V. Gonzalez-Pedro, T. Ripolles-Sanchis, H. P. Wu, L. L. Li, C. Y. Yeh, E. W. G. Diau and J. Bisquert, *J. Phys. Chem. C*, 2011, **115**, 10898–10902.
42 F. Fabregat-Santiago, G. Garcia-Belmonte, I. Mora-Sero and J. Bisquert, *Phys. Chem. Chem. Phys.*, 2011, **13**, 9083–9118.
43 M. C. Beard, G. M. Turner and C. A. Schmuttenmaer, *Phys. Rev. B: Condens. Matter Mater. Phys.*, 2000, **62**, 15764–15777.
44 G. M. Turner, M. C. Beard and C. A. Schmuttenmaer, *J. Phys. Chem. B*, 2002, **106**, 11716–11719.
45 C. A. Schneider, W. S. Rasband and K. W. Eliceiri, *Nat. Methods*, 2012, **9**, 671–675.
46 B. Ferreira, P. F. da Silva, J. S. Seixas de Melo, J. Pina and A. Maçanita, *J. Phys. Chem. B*, 2012, **116**, 2347–2355.
47 M. Belletete, L. Mazerolle, N. Desrosiers, M. Leclerc and G. Durocher, *Macromolecules*, 1995, **28**, 8587–8597.
48 T. N. Murakami, E. Yoshida and N. Koumura, *Electrochim. Acta*, 2014, **131**, 174–183.
49 S. R. Raga, E. M. Barea and F. Fabregat-Santiago, *J. Phys. Chem. Lett.*, 2012, **3**, 1629–1634.
50 A. B. Nepomnyashchii and B. A. Parkinson, *Langmuir*, 2013, **29**, 9362–9368.
51 J. Bisquert, *Phys. Chem. Chem. Phys.*, 2003, **5**, 5360–5364.
52 E. M. Barea, J. Ortiz, F. J. Paya, F. Fernandez-Lazaro, F. Fabregat-Santiago, A. Sastre-Santos and J. Bisquert, *Energy Environ. Sci.*, 2010, **3**, 1985–1994.
53 M. Abrahamsson, P. G. Johansson, S. Ardo, A. Kopecky, E. Galoppini and G. J. Meyer, *J. Phys. Chem. Lett.*, 2010, **1**, 1725–1728.
54 Y. Tamaki, A. Furube, M. Murai, K. Hara, R. Katoh and M. Tachiya, *Phys. Chem. Chem. Phys.*, 2007, **9**, 1453–1460.
55 Y. Tamaki, K. Hara, R. Katoh, M. Tachiya and A. Furube, *J. Phys. Chem. C*, 2009, **113**, 11741–11746.
56 S. E. Koops, P. R. F. Barnes, B. C. O'Regan and J. R. Durrant, *J. Phys. Chem. C*, 2010, **114**, 8054–8061.
57 S. A. Haque, E. Palomares, B. M. Cho, A. N. M. Green, N. Hirata, D. R. Klug and J. R. Durrant, *J. Am. Chem. Soc.*, 2005, **127**, 3456–3462.
58 S. E. Koops, B. C. O'Regan, P. R. F. Barnes and J. R. Durrant, *J. Am. Chem. Soc.*, 2009, **131**, 4808–4818.
59 J. R. Durrant, S. A. Haque and E. Palomares, *Coord. Chem. Rev.*, 2004, **248**, 1247–1257.
60 L. G. C. Rego and V. S. Batista, *J. Am. Chem. Soc.*, 2003, **125**, 7989–7997.
61 C. F. A. Negre, V. C. Fuertes, M. B. Oviedo, F. Y. Oliva and C. G. Sánchez, *J. Phys. Chem. C*, 2012, **116**, 14748–14753.
62 B. O'Regan, L. Xiaoe and T. Ghaddar, *Energy Environ. Sci.*, 2012, **5**, 7203–7215.